sustainability

MDPI

Article

Ultrafast Laser Surface Texturing: A Sustainable Tool to Modify Wettability Properties of Marble

Ana J. López [1,*], Alberto Ramil [1], José S. Pozo-Antonio [2], Teresa Rivas [2] and Dolores Pereira [3]

1 Laboratorio de Aplicacións Industriais do Láser, Centro de Investigacións Tecnolóxicas, Universidade da Coruña, 15471 Ferrol, Spain
2 Departamento de Enxeñaría de Recursos Naturais e Medio Ambiente, Escola de Enxeñaría de Minas e Enerxía, Universidade de Vigo, 36310 Vigo, Spain
3 Department of Geology, Universidad de Salamanca, 37008 Salamanca, Spain
* Correspondence: ana.xesus.lopez@udc.es; Tel.: +34-881-01-3250

Received: 20 June 2019; Accepted: 25 July 2019; Published: 28 July 2019

Abstract: Conservation strategies to reduce the degradation of stone caused by the action of water are focusing on increasing the hydrophobicity of the surface by imitating existing solutions in nature (lotus leafs and others). These are mainly based on the existence of hierarchical roughness with micro- and nanoscale structures. In the case of marble, research has focused on protective coatings that sometimes are dangerous for the health and the environment, and with undesirable effects such as color changes or reduction of water vapor permeability of the stone. Laser texturing, however, is an environmentally friendly technique, because no chemicals or toxic waste are added and, moreover, it can process nearly all types of materials. It has been used to change the surface texture of metals and other materials on a micro or even nanometric scale, to meet a specific functional requirement, such as hydrophobicity. The objective of this work was to analyze the feasibility of this technique to provide hydrophobic properties to a marble surface without appreciable changes in its appearance. Therefore, an analysis of the irradiation parameters with ultra-short-pulse laser was performed. Preliminary results demonstrate the ability of this technique to provide hydrophobic character the marble (contact angles well above 90°). Besides, the analysis of the treated surfaces in terms of roughness, color and gloss indicates that changes in the appearance of the surface are minimal when properly selecting the process parameters.

Keywords: marble; wettability properties; hydrophobicity; laser surface texturing; multiscale roughness; cultural heritage; ultrafast pulse laser

1. Introduction

Marble has been extensively used in historical architecture and monuments owing to its good mineralogical and microstructural properties, durability, and aesthetic quality. However, exposure to the open air for a long time deteriorates the rock surface. In humid climates, biological factors highly contribute to the weathering through physical and chemical interactions that can cause different kinds of alterations, such as the discoloration of materials, the formation of crusts on surfaces, and the loss of material that can lead to structural damage [1]. Particularly calcareous stones are sensitive to the deterioration effects related to water, and the minimization of water contact with calcareous stone surfaces is thus a key aspect in marble conservation [2].

Conservation strategies to reduce the degradation of stone caused by the action of water are being continuously developed. In this sense, new products and procedures have been recently designed to reduce the wetting ability of stone [2–8]. In the case of marble, research has been focused on the development of protective coatings [9–16]. However, some of these coatings include toxic products or processes that are harmful to human health and the environment; in addition, there are other undesirable effects such as color, modifications, or reduction of water vapor permeability above the safe threshold in cultural heritage interventions. In Europe presently, the use of chemicals in these very sensitive environments is scrutinized and regulated by the European Union.

The main index used to evaluate the wettability of a solid surface is the static contact angle, θ, that describes the behavior of a liquid droplet on a solid surface in air, and is defined as the angle between the tangent at the three-phase point and the solid surface. Solid surfaces with $\theta < 90^\circ$ are considered hydrophilic, while surfaces with $\theta > 90^\circ$ are considered hydrophobic [17]. The wetting behavior of a solid surface is driven by the surface free energy at the interfaces between the solid, liquid, and vapor [18]. Expressions for the equilibrium contact angle of a small liquid droplet are given by Young, Wenzel, and Cassie–Baxter for ideal, rough, and composite surfaces, respectively [17,19]. The Wenzel model implies that wettability can be enhanced by increasing the surface roughness:

$$\cos\theta_W = r\,\cos\theta_0 \tag{1}$$

where θ_W is the actual contact angle on rough surface, θ_0 is the contact angle on ideal smooth surface defined by Young's equation, and the Wenzel roughness factor, r, is defined as the ratio of the actual surface area wetted by the liquid and the projected planar area ($r > 1$).

The Wenzel equation is based on the hypothesis that liquid enters grooves present on the surface, leading to a homogeneous wetting regime with increased contact area. This model explains why the contact angle of hydrophilic surfaces decreases with increasing roughness whereas contact angle of hydrophobic surfaces increases. However, Wenzel's model can hardly explain water contact angles exceeding 150° that correspond to super-hydrophobic surfaces. This behavior requires the additional model that was given by Cassie and Baxter. Here, the surface tension dominates the system and it is energetically favorable for the liquid to form a droplet that rests on the tips of the surface while air fills the space between solid and liquid, forming air pockets. Consequently, only a small fraction of the solid surface is in contact with the liquid. The Cassie–Baxter contact angle can be calculated according to

$$\cos\theta_{CB} = -1 + f\,(1 + \cos\theta_0) \tag{2}$$

with $f = \phi/\gamma$; being γ the surface tension and ϕ the fraction of the solid surface which is in contact with the liquid. Therefore, for a given surface composition and liquid, i.e., fixing θ, the nature of the texture (which is determined by r and ϕ) determines the wetting behavior.

There are a large number of published works concerning the functionalization of surfaces to attain special characteristics of wettability for various environmental engineering applications such as self-cleaning, oil–water separation, anti-icing, anti-fouling, corrosion resistance, and food packaging, among others; see for example the review of Barati et al., and references therein [20]. The solutions proposed in these works imitate the hydrophobic structures existing in nature such as lotus leafs, rose petals—in plantae kingdom—and those of arthropod phylum such as structured wings, antifogging and anti-reflective eyes, and structures allowing a shift over water surfaces [21–23]. In all these cases, the hierarchical roughness of biological systems, with micro and nanoscale structures, seems to play a key role in these special properties; so different techniques have been used to emulate these multiscale textures. In the last decade, laser texturing has been widely used [24].

Laser texturing consists of making geometric structures by means of laser ablation processes to change at the relief of the surface to meet a specific functional requirement. The main advantages of laser texturing are: (1) the ability to produce structures on surface areas from microscale to macroscale; (2) the capability of processing non-planar surfaces; (3) a single-step process performed under normal ambient conditions; (4) an eco-friendly process because no chemicals or toxic waste are added to the environment and (5) the ability to process nearly all types of materials. There are several reported works on nano/micro-texturing of different materials such as the improvement of cell adhesion in metallic bio-implants or tribological properties of mechanical components, self-cleaning, corrosion protection, and other applications [25,26]. The lasers used were short-pulse lasers [27–32] as well as ultra-short pulses [31,33–36]. However, the application of laser texturing to modify the wettability of stones is scarce or even nonexistent [37,38].

The aim of this work was to analyze the feasibility of laser texturing as a new and environmentally friendly process, as an alternative to modify the nature of the surface of marble to provide hydrophobic properties without appreciable changes to its appearance. For this purpose, samples of a commercial marble were structured by means of an ultra-short-pulse laser under different irradiation parameters. Two kinds of texturing patterns consisting of matrices of holes and groove arrays were tested, and the most adequate conditions to obtain hydrophobic surfaces were analyzed in detail. The hydrophobicity of the processed marble was assessed by contact angle measurements and the surfaces were also characterized in terms of roughness, color, and gloss to know the changes caused by the texturing process. The results indicate the ability of laser texturing to increase the hydrophobicity of marble so that, after properly selecting the process parameters, changes in the appearance of the surface are minimal.

2. Materials and Methods

2.1. Stone Characterization

For this study, a marble commercially known as Crystal White, from S.R. of Vietnam, was used. Its highly purity on calcite, its homogeneous white color, its equigranular texture, the barely existence of accessory minerals and the absence of veins make this marble very suitable for the purpose of this work. Polished slabs of dimensions 10 cm × 5 cm × 2 cm (length, width and height) were prepared. Geochemical, petrographic and mineralogical characterization of the samples was performed. Chemical composition (whole-rock major and trace elements) was obtained by means Inductively Coupled Plasma-Mass Spectrometry (ICP-MS) using an ICP-MS AGILENT 7800. For this analysis, 0.1 g of sample powder is digested with HNO_3 + HF under pressure in high pressure vessels in Milestone Microwave. Mineralogical composition was obtained by X-ray powder diffraction analysis (Bruker D8 Advance) of bulk rock with CuKa radiation and a velocity of 2θ/min. The equipment used is a Siemens D-500 (40 kV and 30 mA) diffractometer using CuKa radiation ($\lambda = 0.154\,37$ nm) Ni-filter, equipped with the Diffract ATV3 software package. A complete petrographic examination was done following the standard ASTM [39], to describe the mineralogy and textures. A Leica DM2500P microscope under transmitted light was used for this purpose.

2.2. Laser Processing

The laser used was the Spirit system from Spectra Physics with emission wavelength 1040 nm and pulse width $<$ 400 fs. The intensity profile at the laser output was near-Gaussian ($M^2 < 1.2$) and the beam diameter at the exit of the laser head was 1.5 mm. The laser beam presents horizontal polarization ($>$ 100:1). Pulse rate can be selected from single shot to 1 MHz, with maximum pulse energy of 40 µJ at 100 kHz. The maximum mean power output is $>$ 4 W. A two mirror galvanometric scanner (Raylase Superscan

III-15) was used and scanned the laser beam in X–Y directions. The beam was focused by means of a F-theta objective lens, 160 mm focal length, up to a diameter of 30 µm. At the working plane, the beam polarization is parallel to Y direction.

Laser surface treatments were performed in air at atmospheric pressure and two kind of texturing patterns were essayed: matrix of holes and arrays of parallel groves. Hole patterns were obtained through successive laser shoots delivered at the same point of the surface; grooves were obtained by overlapping holes as the laser beam is scanned along X or Y directions.

2.3. Surface Characterization

After laser processing, the samples were analyzed by scanning electron microscopy SEM using a Philips XL30 working in Secondary electrons (SE) mode to obtain a qualitative characterization of the surface. For each sample, 2 cm × 2 cm fragments were carbon coated and visualized with SEM. The optimum conditions of observation were obtained at an accelerating potential of 15–20 kV, a working distance of 9–11 mm and specimen current of ≈ 60 mA.

Then, topographical data were acquired with an optical imaging profiler (Sensofar-PLu 2300) and different objectives were used: a 20× EPI objective, with a field of view of 637 µm × 477 µm and a pixel size of 0.83 µm, and a 100× EPI objective with a field of view of 124 µm × 92 µm and a pixel size of 0.17 µm. Data processing, analysis and visualization were implemented by using Scientific Python. After that, the following roughness parameters were obtained in accordance with standard ISO 25178 [40], related to the analysis of 3D areal surface texture: (1) S_a, mean roughness, is the arithmetic mean of the absolute value of the height from the mean plane of the surface; (2) S_{dr}, developed interfacial area ratio, is a hybrid parameter expressed as the percentage of the definition area's additional surface area contributed by the texture as compared to the planar definition area. This parameter is directly related to the parameter r in Wentzel's equation, owing that $r = 1 + S_{dr}$.

To evaluate the wettability of the textured surfaces, static contact angles were measured with a Phoenix-300 equipped with an automatic dosification system and a 6.5× zoom CCD camera. For each tested surface (included the reference marble), static contact angle of three 4 µL droplet were measured, with a precision of ±0.1°, following sessile drop method EN 828:2013 [41].

Color modifications related to texturing of the marble were evaluated. For this, color characterization before and after texturing was obtained by means of a Minolta CM-700D spectrophotometer equipped with SpectraMagicTM NX software. Color was expressed in the CIELAB and CIELCH spaces [42]. A total of 9 measurements were made for each surface to obtain statically representative results. The measurements were made in Specular Component Included (SCI) mode with a spot diameter of 8 mm, D65 illuminant and an observer angle of 10°. The parameters measured were L^*, the lightness, varying from black (0) to white (100); a^*, which varies from +60 (red) to −60 (green), and b^*, which ranges from +60 (yellow) to −60 (blue). Also, C^*_{ab}, chroma or saturation, and H_{ab}, hue, were measured. Color of the non-textured areas was considered to be the reference to calculate color differences ΔL^*, Δa^*, Δb^*, ΔCab^* and ΔH^* and the global color change, ΔE^*_{ab} ($\Delta E^*_{ab} = \sqrt{(\Delta L^*)^2 + (\Delta a^*)^2 + (\Delta b^*)^2}$).

A glossmeter (Novo Gloss MultiGauge Lite from Neurtek Instruments) was used to obtain the gloss before and after texturing of the marble. Three measurements were performed for each tested surface with a reflection angle of 60°.

3. Results and Discussion

3.1. Surface Characterization

The studied marble has a very similar composition as other marbles (e.g., Carrara marble), [43] very important in cultural heritage and the possible implications of our results in terms of conservation-restoration of the architectural heritage. Crystal White marble has a 51.91% of Ca (expressed as CaO) and a loss on ignition of 42.60%. From ICP-MS data. The largest difference observed with Carrara marble is related to the content of dolomite, as the Crystal White marble is slightly more enriched in this phase than others [43]. This is noticed in the X-ray powder diffraction analyses, where traces of dolomite (magnesium carbonate) have been noticed (Figure 1). In the case of the depth, the most significant variable (very small *p*Value) was the laser power; regarding width, the most significant one was the intercept of the linear fit, which is directly related to the beam spot. The next significant contribution to the width was again the laser power.

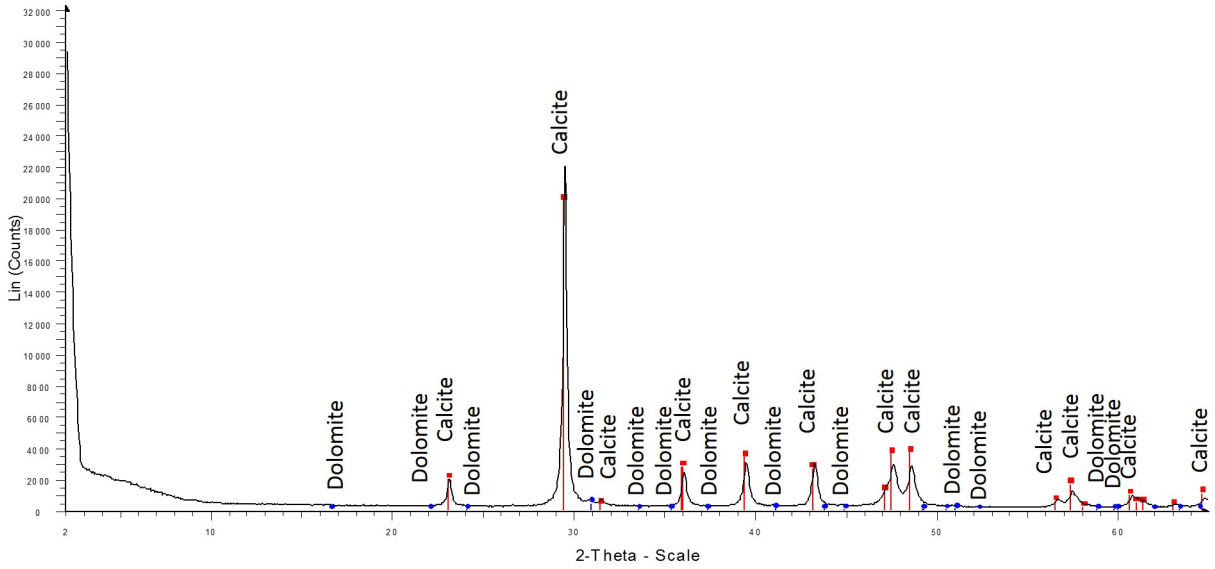

Figure 1. X-ray powder diffraction spectra of the marble selected.

Under petrographic microscopy, the purity of the marble is confirmed as well as the mosaic, granoblastic texture, where individual crystals of calcite meet others with somehow indented boundaries (Figure 2).

3.2. Laser Parameter Analysis

An analysis of the laser processing parameters was performed. The objective was to select the most adequate values to achieve texturing structures that allow the formation of air pockets between the marble surface and the liquid drops, as the Cassie–Baxter model states. The analysis was carried out by means of a multiple linear regression model, which allowed us to determine the sensitivity of the sizes (width and depth) of the structures generated to each of the laser parameters; i.e., pulse frequency, laser power, scanning speed and number of shots (or time of laser shooting).

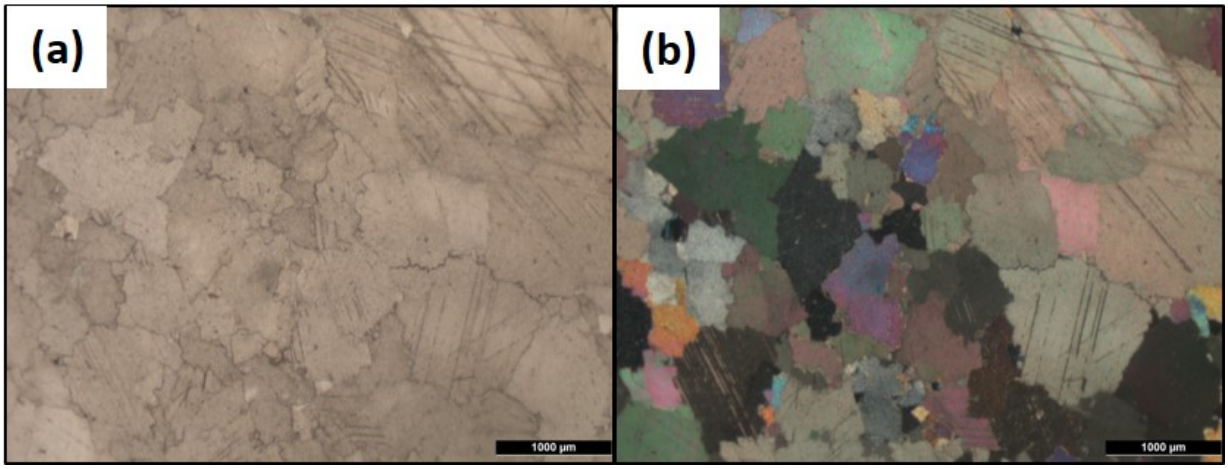

Figure 2. Petrographic micrographs of the Crystal White marble. (**a**) parallel-polarized light, PPL. (**b**) cross-polarized light, CPL.

Owing that the femtosecond laser beam has a Gaussian intensity profile, the profiles of the laser-machined micro-holes will be also like a Gaussian curve. Figure 3 depicts topographic image of a crater and a groove made in the marble surface. Dimensions, depth and width, of these structures were obtained by fitting to a 2D and a 1D Gaussian functions, respectively, the crater and the *X*-axis projection of the groove. Results of the regression analysis, performed by using the dimensions sizes are summarized in Table 1. Regarding depth, the laser power is the most significant variable for both grooves and holes. In case of width, the most relevant contribution is the intercept of the linear fit whose value is near the beam spot size. The next significant variable is again the laser power.

Table 1. Results of Multiple Linear Regression fit for depth and width. SE is the standard error for the coefficient estimates. *p*Value is the null hypothesis probability obtained from Student's *t* distribution. Variables with higher significant result (very small *p*Value) are in bold.

GROOVES				**HOLES**			
Depth = 1 + Freq + Pow + Speed				Depth = 1 + Freq + Pow + Time			
	Estimate	SE	*p*Value		Estimate	SE	*p*Value
(Intercept)	8.2	2.8	1.09×10^{-2}	(Intercept)	8.5	5.7	1.49×10^{-1}
Freq	−0.096	0.030	5.82×10^{-3}	Freq	−0.210	0.063	2.26×10^{-3}
Pow	0.22	0.02	8.21×10^{-9}	**Pow**	0.381	0.053	3.95×10^{-8}
Speed	0.16	0.07	4.49×10^{-2}	Time	−0.00016	0.00090	0.85881
Width = 1 + Freq + Pow + Speed				Width = 1 + Freq + Pow + Time			
	Estimate	SE	*p*Value		Estimate	SE	*p*Value
(Intercept)	24.1	3.0	4.40×10^{-7}	**(Intercept)**	27.1	2.0	2.55×10^{-13}
Freq	−0.073	0.031	3.36×10^{-2}	Freq	−0.003	0.016	8.75×10^{-1}
Pow	0.137	0.021	7.48×10^{-6}	**Pow**	0.081	0.021	5.56×10^{-4}
Speed	0.071	0.075	3.58×10^{-1}	Time	−0.000242	0.000297	4.23×10^{-1}

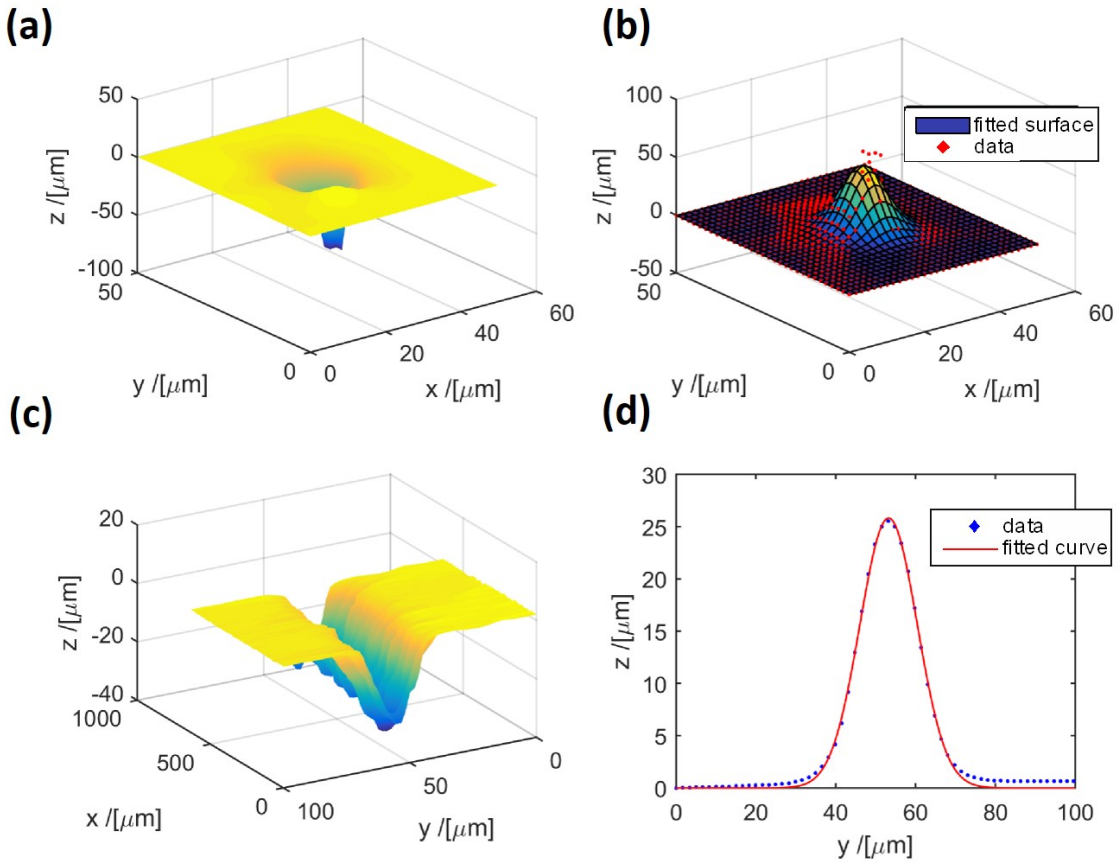

Figure 3. Confocal topographies and fitting results to obtain depth and width dimensions. (**a**) hole topography and (**b**) 2D Gaussian fit. (**c**) groove topography and (**d**) and 1D Gaussian fit.

3.3. Surface Morphology Characterization

The analysis above gave the laser power, P, as the key parameter to control both width and depth of the laser-generated structures. Therefore, in order to investigate the effect of laser power on the surface topography, the marble surface was texturized at a pulse frequency of 50 kHz and laser power ranging from the 100% maximum power, 4 W, to the 40% maximum power, 1.6 W. In the case of textured patterns consisting of a matrix of holes, the time was fixed at 5 ms and, in case of grooves, the scan speed 25 mm s^{-1}. Taking into account the size of the laser spot, ≈ 40 µm, to obtain different textures the pitch (distance between lines or holes) was varied to cover a wide range of structures; from completely separate ones to overlapping. Table 2 shows the texturing parameters used for each configuration (matrix of grooves and matrix of holes).

Table 2. Texturing parameters.

Grooves	Holes
Frequency: 50 kHz	Frequency: 50 kHz
Speed: 25 mm s^{-1}	Time: 5 ms (250 shots)
Power: 100% (4 W), 80%, 60%, 40%	Power: 100% (4 W), 80%, 60%, 40%
Pitch: 20, 30, 40, 50, 60 µm	Pitch: 20, 30, 40, 50, 60 µm

Figure 4 shows SEM micrographs of the laser textured marble at $P = 4$ W, pitch = 60 µm and $P = 4$ W, pitch = 20 µm; performed with grooves and holes. As can be observed, two levels of texture can be differentiated: the form induced by the pattern of grooves or holes (Figure 4a,c,e,g) and, superimposed to this, the roughness that can be seen at higher magnification (Figure 4b,d,f,h). This hierarchical structure, is considered to be a key factor for improving surface hydrophobicity, and has been observed by others researchers in both nanosecond and femtosecond laser texturing processes [27,30,31,44,45].

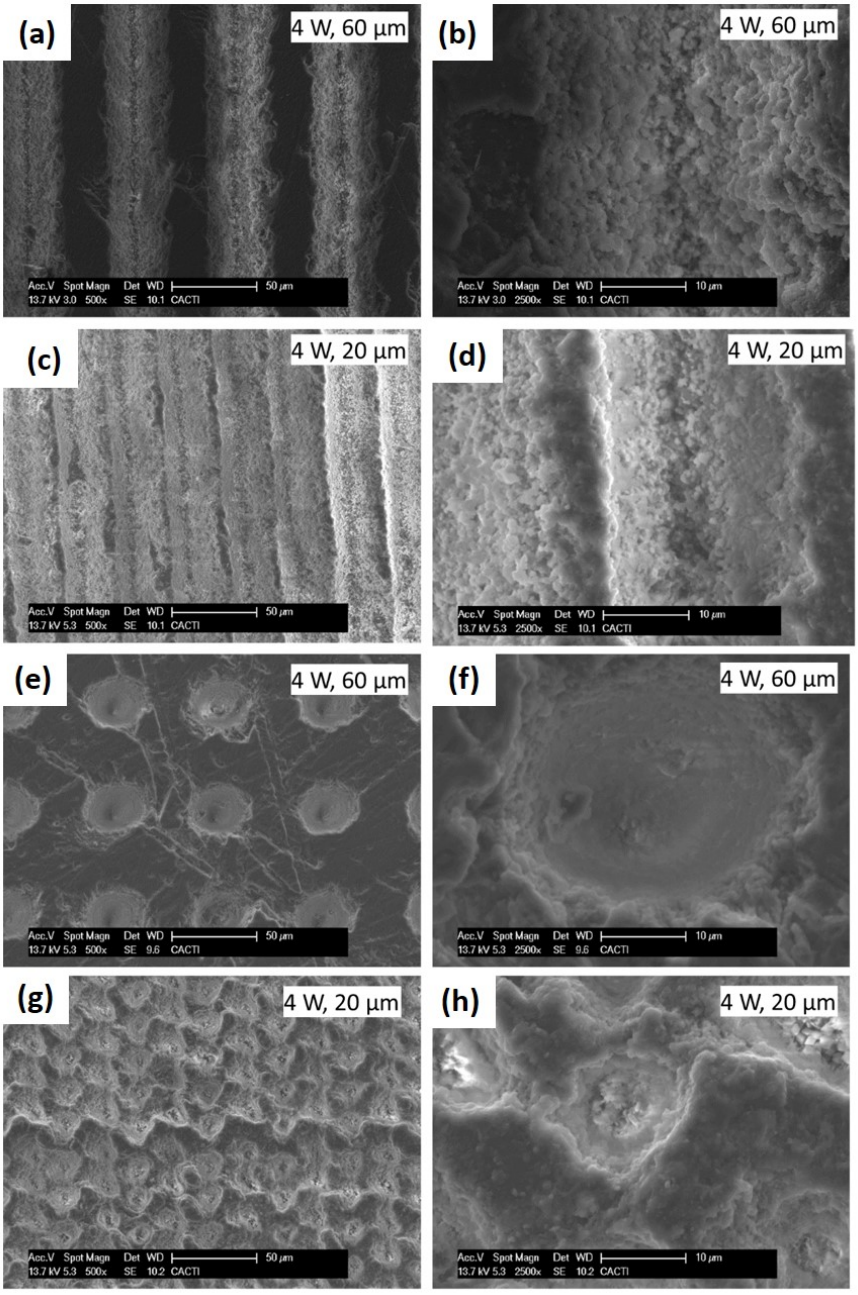

Figure 4. SEM micrographs of some of the laser texturized surfaces treated under different conditions of power and pitch. (**a**–**d**): treated with grooves. (**e**–**h**): treated with holes.

The reconstruction of the surface topography obtained with confocal microscope is shown in Figure 5a,b and transverse profiles of the structures induced, with different pitch, are shown in Figure 5c,d. It can be observed how the texture pattern diffuses with the overlapping, i.e.; decreasing pitch, especially in case of the groove patterns (Figure 5c).

From topographic data, the dimensions of the laser induced structures could be obtained. Figure 6 depicts the values of depth and width which correspond to different values of the processing power. It can be seen that separation is in the order of the laser spot (40 µm), that is the overlap becomes appreciable, the depth of the grooves decreases with the pitch. In the case of the hole patterns, similar trend is observed, although the decrease in depth is not as clear as in the case of the grooves, because the overlap in these structures is lower. Besides, the values show higher dispersion, due to the difficulties to obtain high quality data at the bottom of the holes. Regarding width, values remain practically constant but, again, showing large dispersion, especially in the hole pattern textured with the lowest power, 1.6 W.

Results of the surface roughness parameters S_a and S_{dr} are shown in Figure 7. In the case of the grooves, mean roughness, S_a, seems to increase as the pitch increases, but in the case of holes the opposite occurs; S_a increases as the pitch decreases. This behavior of S_a can be attributed to the increment of the texturing density, while maintaining low overlapping in the generated structures.

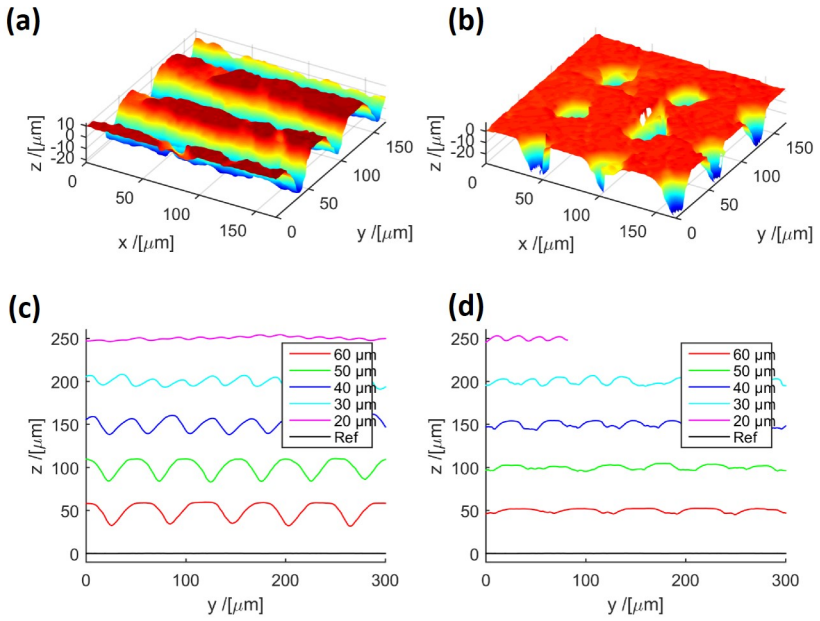

Figure 5. Confocal topographies and profiles of laser texturized surfaces treated under with pitch of 60 µm. (**a**,**c**): treated with grooves. (**b**,**d**): treated with holes.

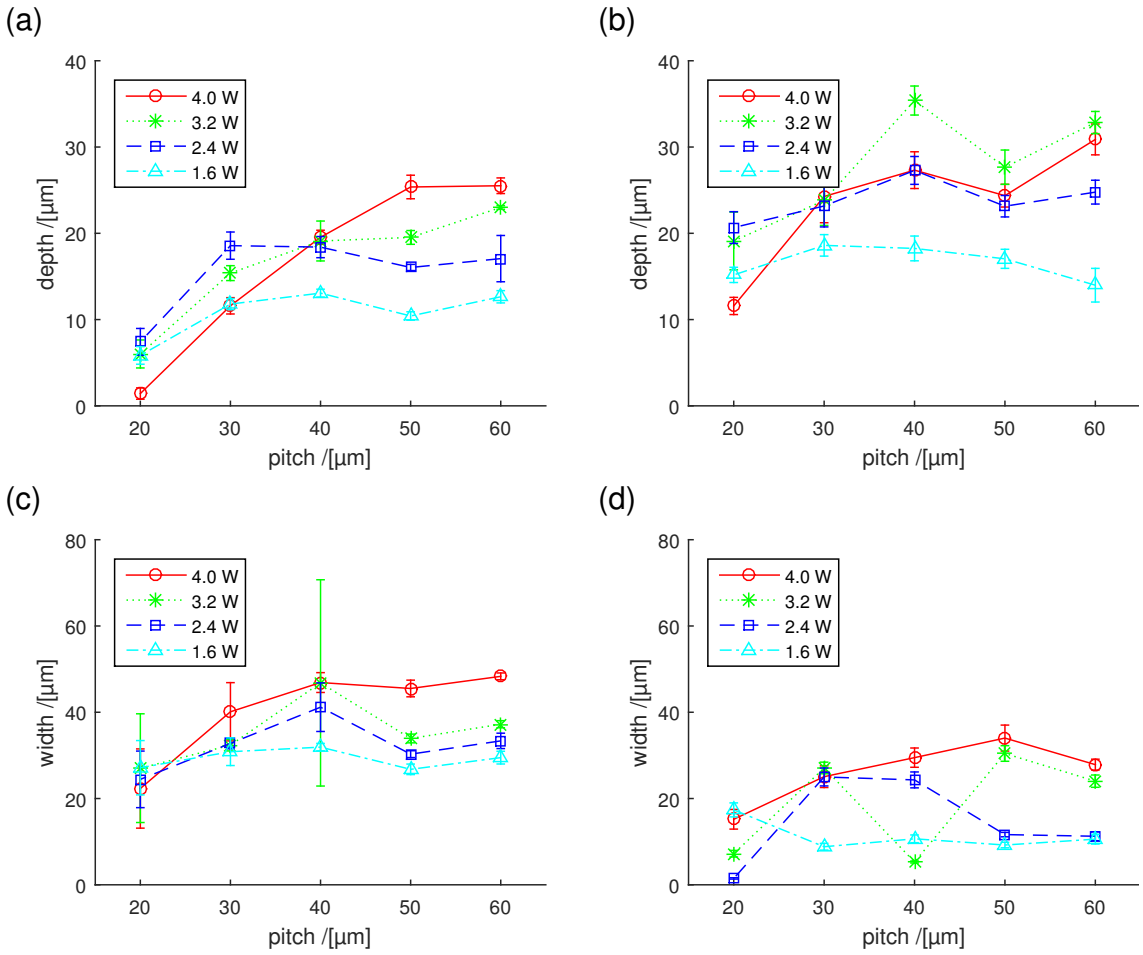

Figure 6. Depth and width versus pitch. (**a**,**c**): treated with grooves. (**b**,**d**): treated with holes.

Regarding S_{dr}, developed interfacial area ratio, this is a more significant parameter from the point of view of the surface wettability. The values obtained, especially in cases of high overlapping, are above the expected ones if only the contribution of the textured density and the overlap, both microscale effects, were considered. These high values of S_{dr} could be attributed to the contribution of the sub-micro scale roughness, which was observed in SEM images of Figure 4. This contribution would increase considerably the textured area with respect to the projected area, thus increasing the S_{dr} values.

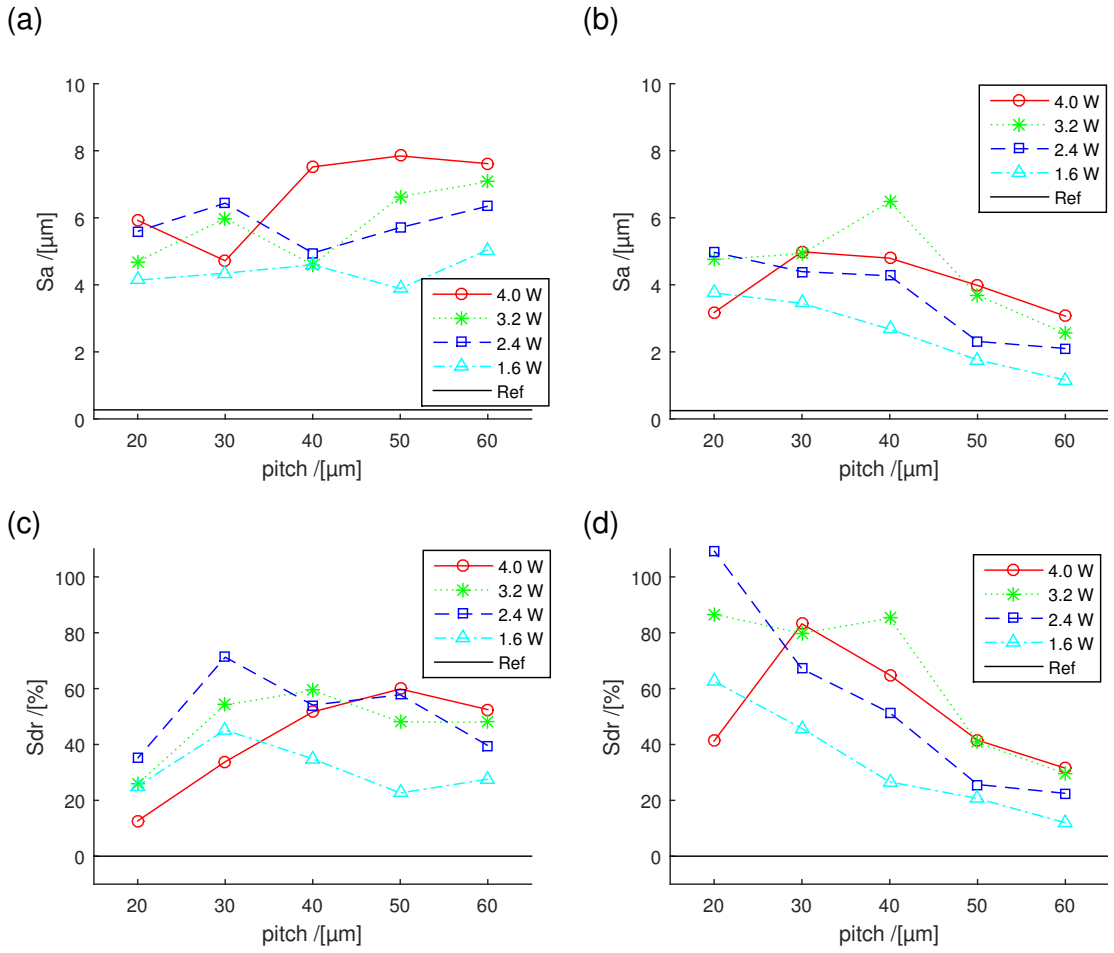

Figure 7. Roughness surface parameters S_a and S_{dr} versus pitch. (**a**,**c**): treated with grooves. (**b**,**d**): treated with holes.

3.4. Wettability

The effect of laser power and pitch on marble wettability was analyzed through the static contact angle, θ. Figure 8 shows the contact angle of the textured surfaces as a function of the pitch, for each value if the laser power used. Gray band corresponds to the static contact angle of the reference marble whose value $\theta_0 = 66.3 \pm 5.8^\circ$ confirms the hydrophilic behavior of this rock. In general terms, after the laser processing, it is observed a significant increase of the contact angles, in most cases well above 90°; that is, the textured marble acquires a clearly hydrophobic character.

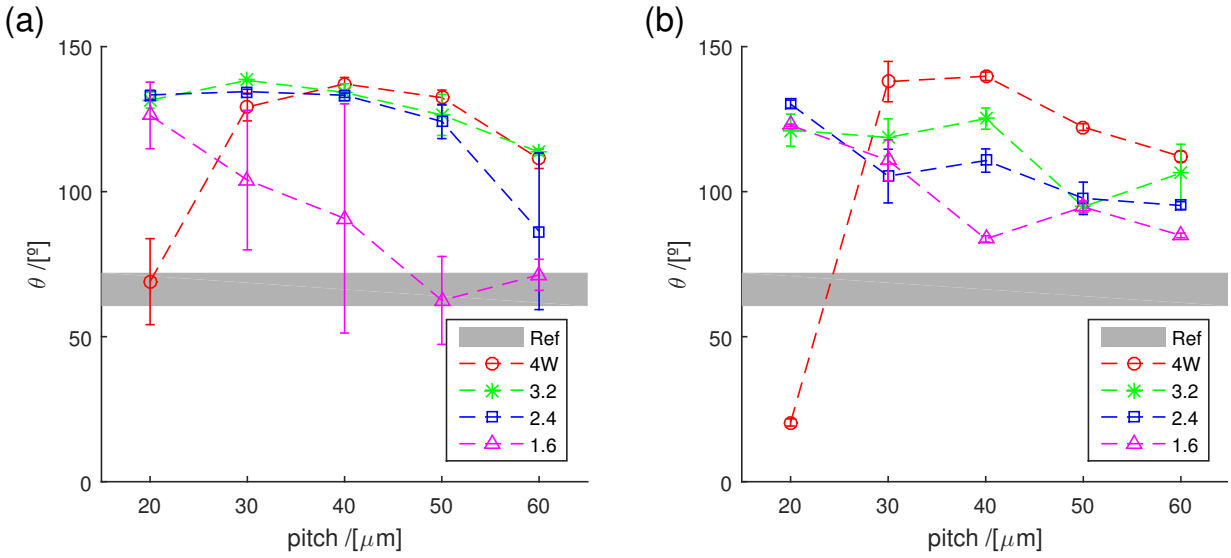

Figure 8. Contact angle of textured surfaces. (**a**): grooves. (**b**): holes.

Focusing on the treatment with grooves, for all the values of the laser power applied (except 1.6 W), the highest contact angles correspond to pitch values in the range 30 µm–50 µm, which correspond to a separation between lines or holes in the order of the laser spot diameter (40 µm). Regarding the case of the lower power used, 1.6 W, the contact angle decreases as the pitch increases; but, it should be taking into account the large dispersion of the data. From Table 3, it can be seen that the power at which the highest contact angle is obtained, corresponds to 3.2 W (30 µm), being $134 \pm 5.5^{\circ}$ the average of the maximum contact angle values obtained with the four laser power used.

Table 3. Power and pitch values, for each texturing pattern (grooves and holes), which give rise to the maximum value of contact angle θ; in addition, the value of ΔE^*_{ab} obtained under each condition is indicated.

	Grooves			**Holes**		
Power	**Pitch**	$\boldsymbol{\theta}$	$\boldsymbol{\Delta E^*_{ab}}$	**Pitch**	$\boldsymbol{\theta}$	$\boldsymbol{\Delta E^*_{ab}}$
4.00	40	137.14	3.50	40	139.79	5.05
3.20	30	138.38	4.31	40	125.18	6.17
2.40	30	134.49	7.91	20	130.18	3.63
2.40	20	133.36	4.53			
1.60	20	126.28	4.16	20	122.90	7.62

With regards of the treatment by holes, in case of $P = 4$ W and $P = 3.2$ W the behavior is similar to the case of grooves, and the highest values of contact angle were obtained in the same pitch range 30 µm–40 µm. However, as can be seen, at $P = 2.4$ W and $P = 1.6$ W, the contact angle decreases as the pitch increases so that the highest values were obtained at the lowest pitch. As a conclusion, the power that obtains the highest contact angle was 4 W (40 µm) and the average value of the maximum contact angles obtained for all the powers tested is $129.0 \pm 7.4^{\circ}$, thus a larger dispersion than in the pattern of grooves was obtained.

3.5. Color and Gloss Changes

Regarding color variations caused by laser texturing, the lightness, L^*, was the most affected parameter, showing increases, in all the textured surfaces, in the range 0.2–7.8 CIELAB units. The color coordinates a^* and b^* did not show notable changes: from -0.16 to 3 in Δa and from 0.6 to 1.7 in Δb. Therefore, nor C^*_{ab} and H^* experimented noticeable changes. Then, global color change (ΔE^*_{ab}) was directly related to L^* variations. In Figure 9, the global color change, ΔE^*_{ab} as a function of the textured pitch, at different values of the laser power are depicted. Moreover, in Table 3, ΔE^*_{ab} values that correspond to the textured patterns which gave the highest contact angles are indicated.

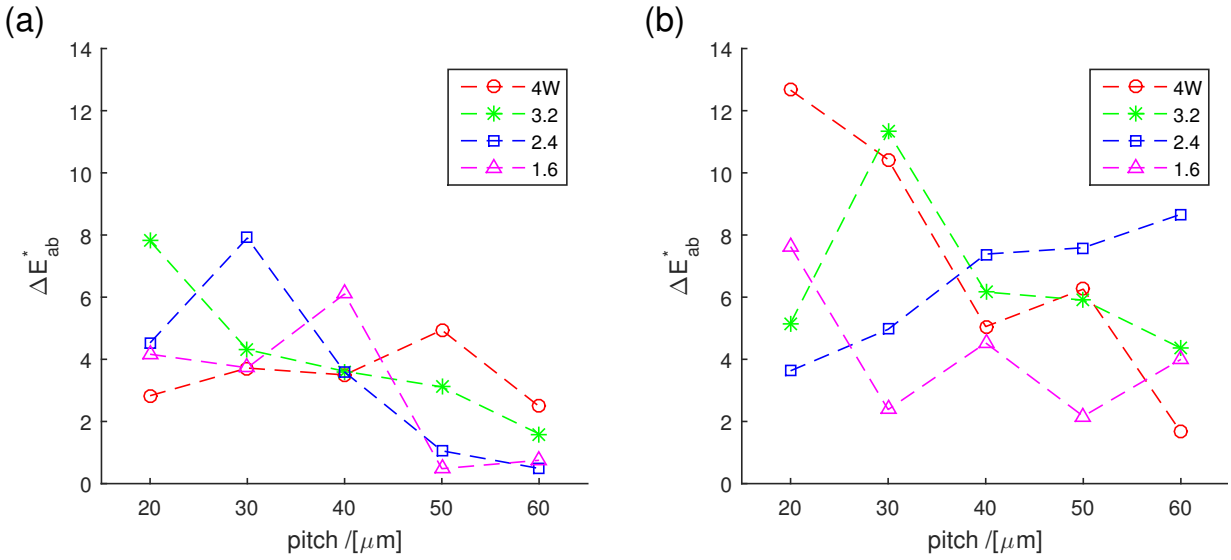

Figure 9. Color difference ΔE^*_{ab} of textured surfaces. (**a**): grooves. (**b**): holes.

Besides, Figure 9 show that neither for groove-type texturing nor for holes-type texturing a clear relationship with pitch can be established; although for groove-type texturing, the lowest values of ΔE^*_{ab} were obtained at the highest pitch, 60 µm. This was an expected result, since the higher the pitch, the lower the textured surface with respect to the original one and, consequently, the potential impact on its color. It is also found that for 60 µm pitch, ΔE^*_{ab} increases with the laser power.

From the literature, it is considered that a global color change ΔE^*_{ab} lower than 3.5 units cannot be observed by an unexperienced human eye [46]. However, it is necessary to interpret color results also from a conservation point of view. In this sense, the rate proposed in [47] was considered. This rate establishes three levels of risk of incompatibility: low risk ($\Delta E^*_{ab} < 3$), medium risk ($3 < \Delta E^*_{ab} < 5$) and high risk ($\Delta E^*_{ab} > 5$).

From the values in Table 3 it can be seen that in surfaces textured with a pattern of holes which lead to the maximum value of contact angle, the color change is higher than in case of grooves; being in all the cases but one, $\Delta E^*_{ab} > 5$ units. Conversely, in grooves-type texturing, ΔE^*_{ab} is always below 5 (this change implies a low to medium risk of incompatibility following [47]), except in the case of 2.4 W; in this case, notice that using a somewhat smaller pitch (20 µm) it was obtained a surface with contact angle just 1° lower and a global color change ΔE^*_{ab} below 5.

Figure 10 shows the gloss values after texturing with grooves and holes applying different laser power and pitch. The value of gloss for the reference surface (gray band in the figure) is 33.25 ± 1.4; this value reflects the polishing finish of the sample. The texturing with both grooves and holes reduces the gloss.

In addition, it is observed, as expected, that the higher the distance between holes or grooves the lower the reduction on the gloss. Furthermore, it can be seen that the laser power applied has a remarkable effect on the gloss; the greater the applied power, the lower the gloss of the textured surfaces.

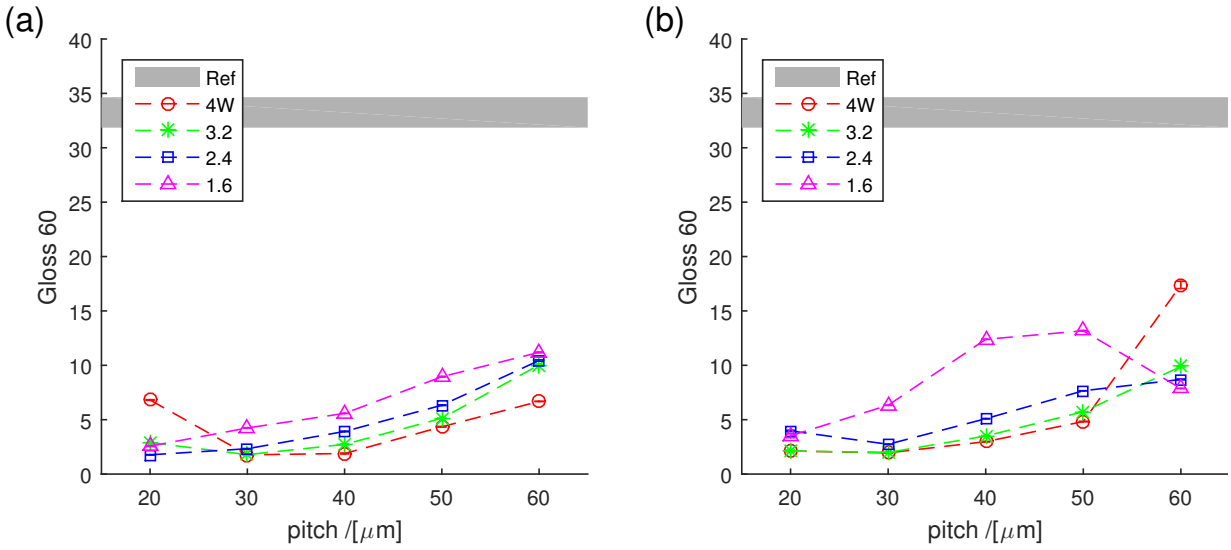

Figure 10. Gloss values of textured surfaces. (**a**): grooves. (**b**): holes.

4. Conclusions

In this work, preliminary results are presented of laser texturing of a marble, a rock widely used in cultural heritage, with hydrophilic character ($\theta = 66.3 \pm 5.8°$), in order to change its wettability characteristics towards an hydrophobic behavior. Surface treatments were performed using a ultra-short-pulse laser and, considering the Cassie–Baxter model of wettability, first an analysis of the irradiation parameters was accomplished to achieve texturing structures that allow the formation of air pockets between the marble surface and the water drops. Therefore, different texturing patterns consisting of matrices of holes and groove arrays were essayed and, from the analysis of irradiation parameters, the laser power has been the most influential variable on the topography of the textured surface, together with the spacing between lines or holes, and pitch, used to fill the surface.

Wettability characteristics of the treated surfaces were measured trough the static contact angle and the results obtained have demonstrated the feasibility of the laser texturing process to modify the marble surface towards a hydrophobic character (contact angle $\theta > 90°$) with, in some cases, values of contact angles close to a super-hydrophobic behavior ($\theta > 150°$). The modification of the wettability depends, however, on the type of structures generated, grooves or holes, the laser power used and the pitch of the texturing patterns. Characterization of areal roughness in terms of the mean roughness, S_a and, especially, the developed interfacial area ratio, S_{dr}, allowed the interpretation of the behavior of the contact angles as a function of the pitch and the power for different texturing patterns. Furthermore, the structured surfaces were evaluated in terms of color parameters and gloss, to detect changes in the appearance of the rock surface that could compromise the aesthetics and, therefore, the applicability of this method in the field of cultural heritage.

The treatment with grooves initially seemed to be the most effective. In this case, values of the contact angle were slightly higher than those obtained with the pattern of holes, and the greatest ones corresponded to pitch in the range 30 µm–50 µm, and they were similar for all the values of the laser power applied ($134 \pm 5.5°$ as the average value). Furthermore, the color changes associated with these texturing

conditions were lower than those obtained with the pattern of holes, and they are below 5 CIELAB units. This value would be associated, according to [47], with a low to medium risk of incompatibility. Nevertheless, according to those authors, the value of the change in any particular property (such as color) of a material used in cultural heritage (such a rock, as was the case) must be interpreted jointly with data on changes in other relevant properties and always in the context of the external conditions (climate, pollution, previous treatments ...) to which this stone will be exposed. Regarding gloss, as was expected, suffered modifications caused by the laser texturing; in this sense, the higher the textured density or the applied power, the lower the surface gloss.

As a conclusion, in this work, we have demonstrated the ability of laser texturing to modify the wettability of marble so that, after properly selecting the process parameters, changes in the appearance of the surface are minimal. One of the next challenges in our research will be the laser texturing of samples with primary cutting surfaces (cut diamond-wire from quarry) or primary sizing (first cut in processing plants of commercial products). This would allow us to incorporate into the study the economic value of laser texturing as an environmentally sustainable alternative stone finishing, with extra properties—hydrophobicity—that would avoid the need to use water-repellent chemicals once the stone is placed on the building.

Author Contributions: The authors confirm contribution to the paper as follows: Conceptualization, A.J.L. and A.R.; methodology, A.J.L., T.R. and D.P.; investigation, A.R., J.S.P.-A., T.R. and D.P.; formal analysis, A.R. and J.S.P.-A.; writing—original draft preparation, A.J.L.; writing—review and editing, A.J.L., A.R., J.S.P.-A., T.R. and D.P.; project administration, A.R.

Funding: This research was funded by the Spanish Ministerio de Economía y Competitividad under grant number BIA2017-85897-R, and the University of Salamanca own financial program.

Conflicts of Interest: The authors declare no conflict of interest.

References

1. Warscheid, T.; Braams, J. Biodeterioration of stone: A review. *Int. Biodeterior. Biodegrad.* **2000**, *46*, 343–368. [CrossRef]
2. Sadat-Shojai, M.; Ershad-Langroudi, A. Polymeric coatings for protection of historic monuments: Opportunities and challenges. *J. Appl. Polym. Sci.* **2019**, *112*, 2535–2551. [CrossRef]
3. Camaiti, M.; Brizi, L.; Bortolotti, V.; Papacchini, A.; Salvini, A.; Fantazzini, P. An Environmental Friendly Fluorinated Oligoamide for Producing Nonwetting Coatings with High Performance on Porous Surfaces. *ACS Appl. Mater. Interfaces* **2017**, *9*, 37279–37288. [CrossRef] [PubMed]
4. Frigione, M.; Lettieri, M.; Frigione, M.; Lettieri, M. Novel Attribute of Organic–Inorganic Hybrid Coatings for Protection and Preservation of Materials (Stone and Wood) Belonging to Cultural Heritage. *Coatings* **2018**, *8*, 319. [CrossRef]
5. Becerra, J.; Mateo, M.; Ortiz, P.; Nicolás, G.; Zaderenko, A.P. Evaluation of the applicability of nano-biocide treatments on limestones used in cultural heritage. *J. Cult. Herit.* **2019**, *38*, 126–135. [CrossRef]
6. Raneri, S.; Barone, G.; Mazzoleni, P.; Alfieri, I.; Bergamonti, L.; De Kock, T.; Cnudde, V.; Lottici, P.P.; Lorenzi, A.; Predieri, G.; et al. Efficiency assessment of hybrid coatings for natural building stones: Advanced and multi-scale laboratory investigation. *Constr. Build. Mater.* **2018**, *180*, 412–424. [CrossRef]
7. Zarzuela, R.; Carbú, M.; Gil, M.A.; Cantoral, J.M.; Mosquera, M.J. CuO/SiO_2 nanocomposites: A multifunctional coating for application on building stone. *Mater. Des.* **2017**, *114*, 364–372. [CrossRef]
8. Quagliarini, E.; Graziani, L.; Diso, D.; Licciulli, A.; D'Orazio, M. Is nano-TiO_2 alone an effective strategy for the maintenance of stones in Cultural Heritage? *J. Cult. Herit.* **2018**, *30*, 81–91. [CrossRef]
9. Aldoasri, M.; Darwish, S.; Adam, M.; Elmarzugi, N.; Ahmed, S.; Aldoasri, M.A.; Darwish, S.S.; Adam, M.A.; Elmarzugi, N.A.; Ahmed, S.M. Protecting of Marble Stone Facades of Historic Buildings Using Multifunctional TiO_2 Nanocoatings. *Sustainability* **2017**, *9*, 2002. [CrossRef]

10. Aldoasri, M.; Darwish, S.; Adam, M.; Elmarzugi, N.; Ahmed, S.; Aldoasri, M.A.; Darwish, S.S.; Adam, M.A.; Elmarzugi, N.A.; Ahmed, S.M. Enhancing the Durability of Calcareous Stone Monuments of Ancient Egypt Using $CaCO_3$ Nanoparticles. *Sustainability* **2017**, *9*, 1392. [CrossRef]
11. Böke, H.; Hale Göktürk, E.; Caner Saltık, E.N. Effect of some surfactants on SO_2–marble reaction. *Mater. Lett.* **2002**, *57*, 935–939. [CrossRef]
12. Matziaris, K.; Panayiotou, C. Tunable wettability on Pendelic marble: Could an inorganic marble surface behave as a "self-cleaning" biological surface? *J. Mater. Sci.* **2014**, *49*, 1931–1946. [CrossRef]
13. Guiamet, P.; Crespo, M.; Lavin, P.; Ponce, B.; Gaylarde, C.; de Saravia, S.G. Biodeterioration of funeral sculptures in La Recoleta Cemetery, Buenos Aires, Argentina: Pre- and post-intervention studies. *Colloids Surfaces B Biointerfaces* **2013**, *101*, 337–342. [CrossRef] [PubMed]
14. Tsakalof, A.; Manoudis, P.; Karapanagiotis, I.; Chryssoulakis, I.; Panayiotou, C. Assessment of synthetic polymeric coatings for the protection and preservation of stone monuments. *J. Cult. Herit.* **2007**, *8*, 69–72. [CrossRef]
15. Cámara, B.; de Buergo, M.Á.; Bethencourt, M.; Fernández-Montblanc, T.; La Russa, M.F.; Ricca, M.; Fort, R. Biodeterioration of marble in an underwater environment. *Sci. Total Environ.* **2017**, *609*, 109–122. [CrossRef] [PubMed]
16. Kronlund, D.; Lindén, M.; Smått, J.H. A sprayable protective coating for marble with water-repellent and anti-graffiti properties. *Prog. Org. Coat.* **2016**, *101*, 359–366. [CrossRef]
17. Bico, J.; Thiele, U.; Quéré, D. Wetting of textured surfaces. *Colloids Surfaces A Physicochem. Eng. Asp.* **2002**, *206*, 41–46. [CrossRef]
18. de Gennes, P.G. Wetting: Statics and dynamics. *Rev. Mod. Phys.* **1985**, *57*, 827–863. [CrossRef]
19. Bico, J.; Marzolin, C.; Quéré, D. Pearl drops. *Europhys. Lett. (EPL)* **1999**, *47*, 220–226. [CrossRef]
20. Barati Darband, G.; Aliofkhazraei, M.; Khorsand, S.; Sokhanvar, S.; Kaboli, A. Science and Engineering of Superhydrophobic Surfaces: Review of Corrosion Resistance, Chemical and Mechanical Stability. *Arab. J. Chem.* **2018**. [CrossRef]
21. Darmanin, T.; Guittard, F. Superhydrophobic and superoleophobic properties in nature. *Mater. Today* **2015**, *18*, 273–285. [CrossRef]
22. Zhang, M.; Feng, S.; Wang, L.; Zheng, Y. Lotus effect in wetting and self-cleaning. *Biotribology* **2016**, *5*, 31–43. [CrossRef]
23. Fadeeva, E.; Chichkov, B.; Fadeeva, E.; Chichkov, B. Biomimetic Liquid-Repellent Surfaces by Ultrafast Laser Processing. *Appl. Sci.* **2018**, *8*, 1424. [CrossRef]
24. Müller, F.; Kunz, C.; Gräf, S.; Müller, F.A.; Kunz, C.; Gräf, S. Bio-Inspired Functional Surfaces Based on Laser-Induced Periodic Surface Structures. *Materials* **2016**, *9*, 476. [CrossRef] [PubMed]
25. Lutey, A.H.A.; Gemini, L.; Romoli, L.; Lazzini, G.; Fuso, F.; Faucon, M.; Kling, R. Towards Laser-Textured Antibacterial Surfaces. *Sci. Rep.* **2018**, *8*, 10112. [CrossRef] [PubMed]
26. Wahab, J.A.; Ghazali, M.J.; Yusoff, W.M.; Sajuri, Z. Enhancing material performance through laser surface texturing: A review. *Trans. Inst. Met. Finish.* **2016**, *94*, 193–198. [CrossRef]
27. Fiorucci, M.P.; López, A.J.; Ramil, A. Comparative study of surface structuring of biometals by UV nanosecond Nd:YVO4 laser. *Int. J. Adv. Manuf. Technol.* **2014**, *75*, 515–521. [CrossRef]
28. Lutey, A.H.A.; Romoli, L. Pulsed laser ablation for enhanced liquid spreading. *Surf. Coat. Technol.* **2019**, *360*, 358–368. [CrossRef]
29. Cai, Y.; Chang, W.; Luo, X.; Sousa, A.M.; Lau, K.H.A.; Qin, Y. Superhydrophobic structures on 316L stainless steel surfaces machined by nanosecond pulsed laser. *Precis. Eng.* **2018**, *52*, 266–275. [CrossRef]
30. Jagdheesh, R.; García-Ballesteros, J.J.; Ocaña, J.L. One-step fabrication of near superhydrophobic aluminum surface by nanosecond laser ablation. *Appl. Surf. Sci.* **2016**, *374*, 2–11. [CrossRef]
31. Huerta-Murillo, D.; García-Girón, A.; Romano, J.M.; Cardoso, J.T.; Cordovilla, F.; Walker, M.; Dimov, S.S.; Ocaña, J.L. Wettability modification of laser-fabricated hierarchical surface structures in Ti-6Al-4V titanium alloy. *Appl. Surf. Sci.* **2019**, *463*, 838–846. [CrossRef]
32. Riveiro, A.; Soto, R.; Del Val, J.; Comesaña, R.; Boutinguiza, M.; Quintero, F.; Lusquiños, F.; Pou, J. Texturing of polypropylene (PP) with nanosecond lasers. *Appl. Surf. Sci.* **2016**, *374*, 379–386. [CrossRef]

33. Arenas, M.; Ahuir-Torres, J.; García, I.; Carvajal, H.; de Damborenea, J. Tribological behaviour of laser textured Ti6Al4V alloy coated with MoS2 and graphene. *Tribol. Int.* **2018**, *128*, 240–247. [CrossRef]
34. Rukosuyev, M.V.; Lee, J.; Cho, S.J.; Lim, G.; Jun, M.B.G. One-step fabrication of superhydrophobic hierarchical structures by femtosecond laser ablation. *Appl. Surf. Sci.* **2014**, *313*, 411–417. [CrossRef]
35. Moradi, S.; Kamal, S.; Englezos, P.; Hatzikiriakos, S.G. Femtosecond laser irradiation of metallic surfaces: Effects of laser parameters on superhydrophobicity. *Nanotechnology* **2013**, *24*, 415302. [CrossRef] [PubMed]
36. Rajab, F.H.; Liauw, C.M.; Benson, P.S.; Li, L.; Whitehead, K.A. Picosecond laser treatment production of hierarchical structured stainless steel to reduce bacterial fouling. *Food Bioprod. Process.* **2018**, *109*, 29–40. [CrossRef]
37. Chantada, A.; Penide, J.; Pou, P.; Riveiro, A.; del Val, J.; Quintero, F.; Soto, R.; Lusquiños, F.; Pou, J. Laser surface texturing of granite. *Procedia Manuf.* **2017**, *13*, 687–693. [CrossRef]
38. Chantada, A.; Penide, J.; Riveiro, A.; del Val, J.; Quintero, F.; Meixus, M.; Soto, R.; Lusquiños, F.; Pou, J. Increasing the hydrophobicity degree of stonework by means of laser surface texturing: An application on Zimbabwe black granites. *Appl. Surf. Sci.* **2017**, *418*, 463–471. [CrossRef]
39. ASTM International. *ASTM C1721—15 Standard Guide for Petrographic Examination of Dimension Stone*; Technical Report; ASTM International: West Conshohocken, PA, USA, 2015. [CrossRef]
40. International Organisation of Standardization. *ISO 25178 Geometric Product Specifications (GPS)—Surface Texture: Areal*; International Organisation of Standardization: Geneva, Switzerland, 2010.
41. AENOR. *UNE-EN 828: 2013—Adhesives - Wettability - Determination by measurement of contact angle and surface free energy of solid surface*; Technical Report; AENOR: Madrid, Spain, 2013.
42. CIE S014-4/E. *2007 Colorimetry—Part 4: CIE 1976 L*a*b* Colour Space*; Technical Report, Commission Internationale de l'Eclairage; CIE Central Bureau: Vienna, Austria, 2007.
43. Herz, N.; Dean, N.E. Stable isotopes and archaeological geology: The Carrara marble, northern Italy. *Appl. Geochem.* **1986**, *1*, 139–151. [CrossRef]
44. Fiorucci, M.P.; López, A.J.; Ramil, A. Multi-scale characterization of topographic modifications on metallic biomaterials induced by nanosecond Nd:YVO 4 laser structuring. *Precis. Eng.* **2018**, *53*, 163–168. [CrossRef]
45. Zheng, B.; Jiang, G.; Wang, W.; Mei, X. Fabrication of superhydrophilic or superhydrophobic self-cleaning metal surfaces using picosecond laser pulses and chemical fluorination. *Radiat. Eff. Defects Solids* **2016**, *171*, 461–473. [CrossRef]
46. Mokrzycki, W.; Tatol, M. Colour difference δE—A survey. *Mach. Graph. Vis.* **2011**, *20*, 383–411.
47. Rodrigues, J.D.; Grossi, A. Indicators and ratings for the compatibility assessment of conservation actions. *J. Cult. Herit.* **2007**, *8*, 32–43. [CrossRef]